CLIMA 2016 - proceedings of the 12th REHVA World Congress

volume 5

Heiselberg, Per Kvols

Publication date:
2016

Document Version
Publisher's PDF, also known as Version of record

Experimental Investigation of a Turbulent Free Jet in Ducts with Single Wall Openings and Gradient Rectangular Cross-Sections

Henning Freitag[#1], Paul Mathis[#2], Dirk Müller[#3]

[#]*E.ON Energy Research Center, Institute for Energy Efficient Buildings and Indoor Climate, RWTH Aachen University*
Mathieustr. 10, 52074 Aachen, Germany

[1]hfreitag@eonerc.rwth-aachen.de

[2]pmathis@eonerc.rwth-aachen.de

[3]dmueller@eonerc.rwth-aachen.de

Abstract
An experimental study on the entrainment behavior of a single turbulent free jet in a duct with a single side wall opening is presented in this paper. Entrainment opening area, diffusor angle of the duct and pressure drop of the entrained air mass flow are varied in order to investigate the influence on the entrained air mass flow. Entrainment increases non-linearly with increasing entrainment opening area. Maximum entrainment is found for small duct diffusor angles, increasing with larger opening areas. Entrainment decreases linearly using small entrainment opening areas and non-linearly using larger entrainment opening areas for higher diffusor angles whereupon a different wall attachment behavior of the jet can be observed using particle image velocimetry (PIV) measurement results. For given entrainment air flow resistances entrainment rates increase with nozzle Reynolds number.

Keywords - active chilled beam; turbulent jet; entrainment; particle image velocimetry

1. Introduction

Active chilled beams (ACB) are used to simultaneously ventilate and cool or heat indoor spaces. The characteristic feature of these devices is the entrainment of air due to turbulent mixing at the jet edges of multiple small, high velocity primary air jets which are located inside the device. This entrainment causes room air to be drawn into the chilled beam where it is cooled or heated according to the occupants' needs by passing a heat exchanger with a set water temperature. Usually, the air is entrained from a defined direction perpendicular to the primary air jet axis through a defined opening causing the jets to deform and to deflect. Mixing of the primary and the entrained air takes place in a duct further downstream before the mixed air exits the active chilled beam into the room.

Assuming a constant temperature difference between water supply and room air the thermal power of the active chilled beam depends on the entrainment ratio (or induction ratio) $I_e = \dot{m}_{sec}/\dot{m}_{prim}$ meaning the ratio

between the mass flow rate of the entrained secondary air $\dot{m}_{sec}$ and the supplied primary air $\dot{m}_{prim}$. Main influences on the entrainment ratio are the beam's internal geometry or additional flow losses, as due to a heat exchanger, for example. The general characteristics of the internal air flow of a fixed, generic ACB geometry with multiple nozzles and without heat exchanger have been investigated in an experimental study by Freitag et al. [1] and in a simulative study by Koskela et al. [2] in order to understand the relevant physical effects better. It was shown that computationally expensive turbulence modeling in the form of large eddy simulations (LES) is necessary to predict the airflow correctly. Thus, an empirical optimization approach was chosen using a variable, generic ACB geometry with a single nozzle. First experimental results on the influence of the ACB's secondary air opening width on the entrainment ratio have been presented in Mathis et al. [3].

In this paper, impacts of three factors influencing the entrainment ratio are investigated experimentally. Firstly, the area of the rectangular entrainment opening is varied by altering the opening length in the jet flow direction. Secondly, the duct geometry is varied with respect to the streamwise cross-section by altering the bottom wall to form a diffusor outlet. Thirdly, the pressure drop in the entrainment air inlet is varied to account for different heat exchanger flow resistances.

2. Methods

Measurements were conducted using an experimental setup containing an optically accessible, generic geometry of an active chilled beam with a single nozzle. Geometry and dimensions of the duct are shown in Fig. 1 including the measurement plane of the PIV measurements.

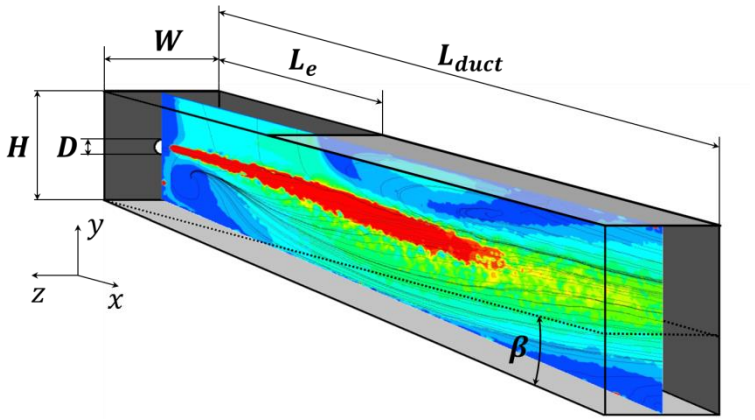

Fig. 1 Dimensions and coordinates used in the duct and PIV light sheet position showing a mapped exemplary contour plot of the planar velocity distribution

The primary air jet emerges from a single nozzle with a quarter circle shaped rounded inlet and a sharp exit with diameter D. The nozzle is centered in a square wall of constant width W and height H. Four rigid walls are used to form the duct downstream the nozzle. Front and bottom wall are made of glass to ensure good optical properties and robustness. The top wall is made of transparent PMMA and tailored to fit in a guide profile in order to be able to move the wall in the x-direction to form an entrainment opening with a variable length L_e. The back wall is made of PVC and coated with matt black color to minimize optical reflections. All surfaces are smooth and flush with the adjacent walls to minimize gap spacing. The bottom wall is pivot-mounted and can be tilted to adjust the bottom wall angle β, with $\beta = 0$ being the case where bottom and top wall are aligned parallel to each other. By this, the duct height $H(x)$ is linearly dependent on x to form a duct with gradient rectangular cross-sections and $\mathrm{d}H/\mathrm{d}x > 0$ for all diffusor geometries.

Functional components of the experimental setup are shown schematically in Fig. 2. A compressed air connection and a high-precision thermal mass flow controller (Vögtlin Instruments red-y smart series) were used to supply the nozzle with a defined mass flow of primary air. An air distribution chamber and a flow straightener are placed upstream the nozzle to ensure non-rotational, even outflow conditions and a reproducible static pressure measurement.

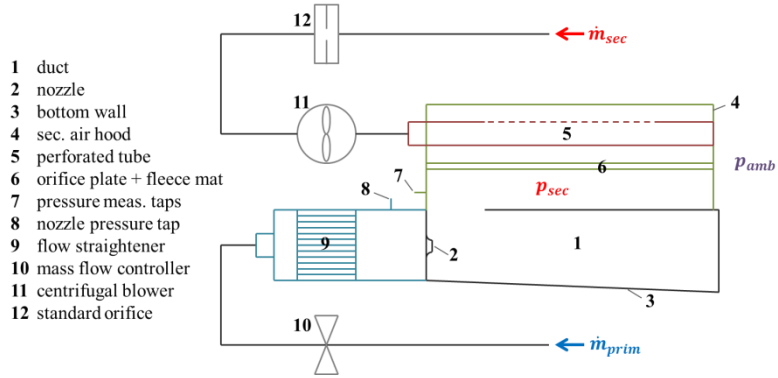

Fig. 2 Schematic of the experimental setup's components

Secondary air flow rates were determined using the differential pressure method with an ISO 5167 standard orifice and a downstream variable speed centrifugal blower. A hood was installed on top of the duct and made airtight against the environment to ensure only the secondary air mass flow is entrained and entering the duct. A perforated supply tube, an orifice plate and a textile mat were used to homogenize the velocity profile upstream the entrainment opening. In order to determine the instantaneous entrainment

rate the static pressure difference $\Delta p = p_{sec} - p_{amb}$ between the secondary and ambient air was measured using a differential pressure sensor (Sensirion SDP1000-L025). Multiple pressure taps were installed 20 mm above the entrainment opening and connected by an annular tube. According to the set value of Δp the speed of the blower was controlled by industrial controlling hardware (ICP DAS ET-87Pn series components) and a corresponding control program running in LabVIEW. The minimum entrainment pressure difference Δp_{min} is determined when the secondary air pipe is sealed and the blower speed is zero.

Flow fields were measured in the x,y-symmetry plane by two-dimensional, two component (2D2C) particle image velocimetry (PIV) using a pulsed Nd:YAG laser (Quantel EverGreen 200), a 5.5 MPixel sCMOS camera (Andor Neo 5.5) and a synchronizing unit (BNC Model 575). Liquid DEHS nebulized in an aerosol generator (Palas AGK2000) was used as particle seeding. A Scheimpflug setup was used for image acquisition to take into account non-perpendicular viewing angles between the laser light sheet and the optical axis. Detailed information on the PIV method can be found in the literature [4].

All measurements were conducted under isothermal conditions. Air temperatures, absolute pressure and relative humidity were measured to determine the secondary air mass flow and air viscosity. Error estimation was conducted to account for specified uncertainties of the measurement equipment which was used in the experiment. In Fig. 3 exemplary measurement values are used to display the relative uncertainty for a fixed entrainment opening area of $L_e/D = 20$.

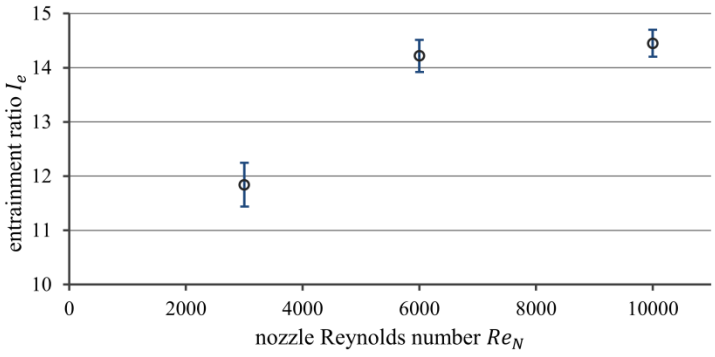

Fig. 3 Estimated entrainment ratio measurement uncertainty for $L_e/D = 20$

Relative measurement uncertainties are higher for smaller primary air mass flow rates (approx. 2.8% for $Re_N = 3000$) than for higher ones (approx. 1.6% for $Re_N = 10000$). Actual repeatability of the measured values is

superior to the uncertainty since all measurement values are time averaged over a period of 30 s offering a sufficient accuracy for qualitative evaluation of the results.

3. Results and Discussion

3.1 Influence of the entrainment opening area

Measurements were conducted for three different primary air mass flows resulting in Reynolds numbers Re_N of 3000, 6000 and 10000 based on the nozzle diameter D. Self-similarity of the primary air jet can be observed for $Re_N \geq 6000$. However, results are fluctuant for $Re_N = 3000$ as the momentum of the primary air jet is low and control of the pressure dependent values becomes more erratic.

The area of the rectangular entrainment opening is varied by altering the opening length L_e while the entrainment ratio I_e is measured. Results are shown in Fig. 4.

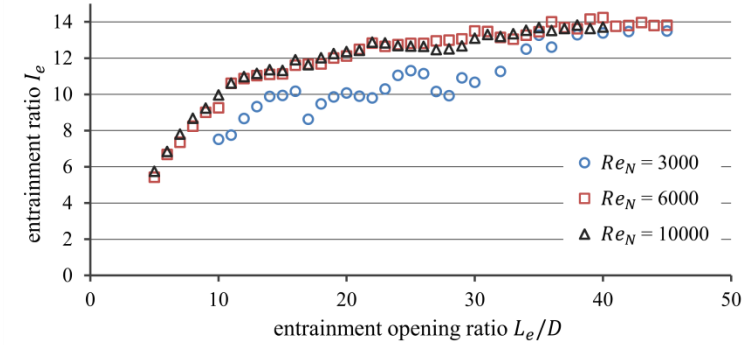

Fig. 4 Influence of the entrainment opening area on the entrainment ratio for three different nozzle exit velocities and $\beta = 0°$

For small values of L_e the entrainment of secondary air is hindered due to a small opening area. The entrainment ratio increases continuously over the measurement range when L_e is increased. However, different gradients can be observed with a strong increase for values of $L_e/D < 11$ and a change to a smaller gradient for values of $L_e/D > 12$.

3.2 Influence of the diffusor angle of the duct

The duct geometry is varied with respect to the streamwise cross-section by altering the bottom wall angle to form a diffusor-shaped outlet using values $\beta > 0°$. Results for $Re_N = 10000$ are shown in Fig. 5.

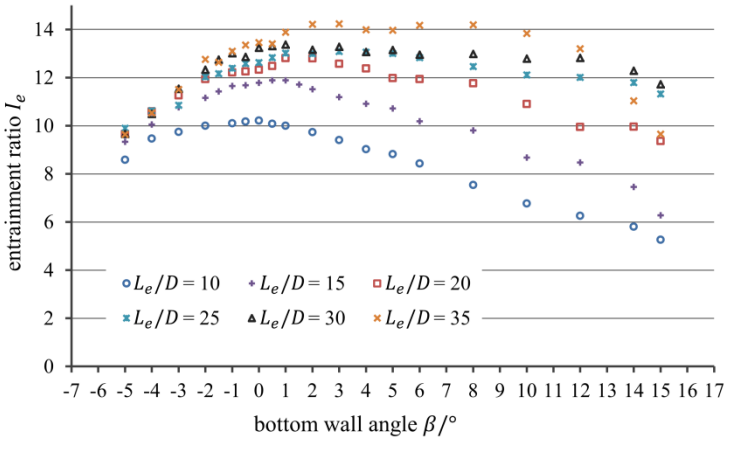

Fig. 5 Influence of the duct bottom wall angle on the entrainment ratio for varying L_e/D and $Re_N = 10000$

As discussed previously, more secondary air is entrained when the entrainment opening area L_e/D is increased. When increasing the bottom wall angle gradually, starting from $\beta = -5°$ entrainment ratios increase until a maximum is reached and values decrease again for larger values of β. Two characteristics can be observed when L_e/D is increased. Firstly, the angle of maximum entrainment is rising from approx. $\beta = 0°$ for $L_e/D = 10$ to approx. $\beta = 3°$ for $L_e/D = 35$. Secondly, entrainment ratios become increasingly stable for increasing values of L_e/D resulting in a range of maximum entrainment rather than showing a linear decay after reaching the peak value. For $L_e/D = 30$, for example, I_e remains constant for approx. $2° < \beta < 8°$.

According to the continuity equation the mean velocity of the flow in the x direction is lower due to a larger cross-section in cases of diffusor shaped ducts. The flow is decelerated resulting in a static pressure gain. Since the jet expands to the ambient pressure in all cases higher values of the entrainment ratio in cases of small diffusor angles can be reached. Flow separation and unwanted entrainment of ambient air counteracts the advantage of the diffusor leading to momentum loss and lower entrainment ability of the jet.

The planar (u,v) velocity distribution for velocity components in the (x,y) symmetry plane (z = 0), respectively, is shown in Fig. 6. In a qualitative comparison of three different values of β (0° (a), 1° (b), 10° (c)) it can be observed that flow patterns (a) and (b) are similar for approx. $x/D < 15$. No significant differences can be found in the comparison of flow pattern (a) and (b) although the measured entrainment rate is approx. 4 % higher for case

(b). Momentum decay is highest for larger angles resulting in lower velocities in case (c) for $x/D > 15$. A broadening of the jet, a smaller jet deflection angle and a smaller recirculation area at the top wall are visible. Additionally, a separation of the jet from the bottom wall can be found at approx. $x/D = 15$ in case (c).

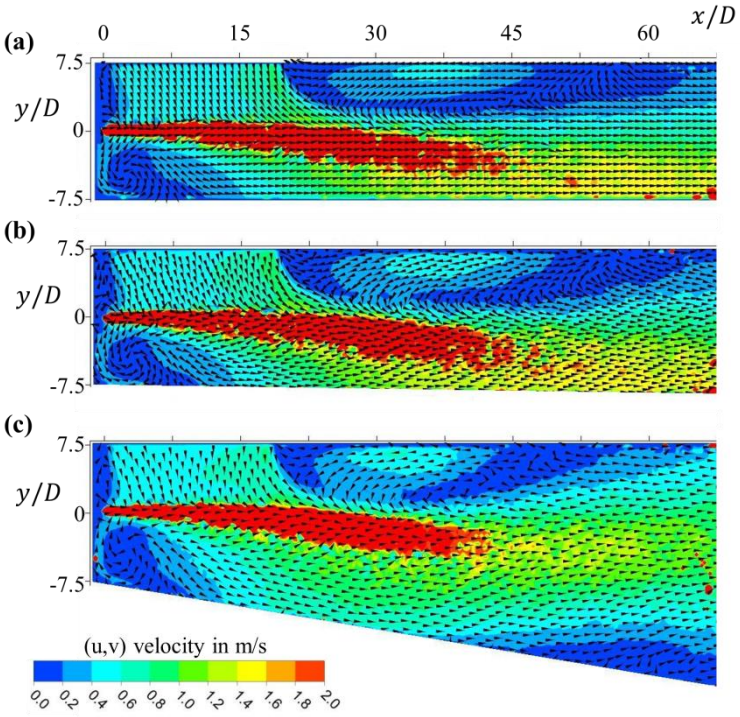

Fig. 6 Contour and vector plot of the planar velocity in the symmetry plane (z = 0) for $L_e/D = 20$ and $Re_N = 10000$ with cases $\beta = 0°$ (a), $\beta = 1°$ (b) and $\beta = 10°$ (c)

3.3 Influence of the secondary air inlet pressure drop

The pressure drop in the entrainment air inlet is varied virtually by adjusting the set value of the pressure difference Δp between the secondary and ambient air to account for different heat exchanger flow resistances. In Fig. 7 the influence of Δp on I_e is displayed for a fixed entrainment opening $L_e/D = 20$, a bottom wall angle of $\beta = 0°$ and three different primary air mass flows resulting in Reynolds numbers Re_N of 3000, 6000 and 10000 based on the nozzle diameter D.

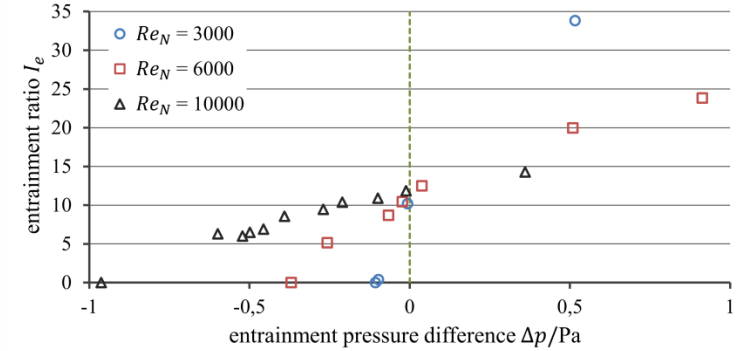

Fig. 7 Influence of the entrainment air inlet pressure on the entrainment ratio for L_e/D = 20 and $\beta = 0°$

It can be stated that the entrainment ratio is only independent from the nozzle Reynolds number in the case of $\Delta p = 0$ (dashed line), i.e. when the secondary air is entrained without further flow resistances. Results for virtual pressure resistances like a heat exchanger, for example, are displayed for $\Delta p < 0$ Pa. Due to higher momentum of the jet the minimum entrainment pressure difference Δp_{min} becomes smaller for higher nozzle Reynolds numbers. For cases not relevant to the application $\Delta p > 0$ and air is actively blown into the ACB through the entrainment opening resulting in larger entrainment ratios for decreasing Reynolds numbers.

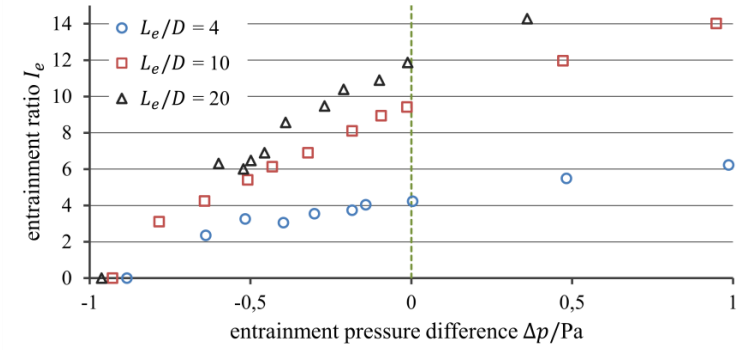

Fig. 8 Influence of the entrainment air inlet pressure on the entrainment ratio for Re_N = 10000 and $\beta = 0°$

When varying the opening area at a constant nozzle Reynolds number the minimum entrainment pressure difference Δp_{min} is nearly independent from L_e/D, as shown in Fig. 8. Small variations of Δp_{min} originate from

different shapes of the recirculation vortex at the top wall due to different values of L_e, presumably.

4. Conclusions and Outlook

It can be concluded that the entrainment behavior of a single jet in a generic geometry of an active chilled beam can be optimized by geometrical values like the entrainment opening area and the diffusor angle of the supply duct. However, optimal geometry values are dependent on factors limiting the upstream entrainment air supply like the pressure resistance of a heat exchanger, for example. PIV measurements are valuable in order to gain insight into relevant factors influencing the induction behavior and can be used to validate numerical simulation data. Ultimately, valid computational models are needed for the development of application oriented ACB geometries with improved performance.

Acknowledgment

Grateful acknowledgment is made for financial support by BMWi (German Federal Ministry of Economics and Technology), promotional reference 03ET1092B.

References

[1] H. Freitag, M. Schmidt, D. Müller, H. Koskela, P. Mustakallio. Particle image velocimetry measurements of the internal air flow in active chilled beams, Roomvent 2014, Sao Paolo, Brazil, October 2014.

[2] H. Koskela, P. Saarinen, H. Freitag, M. Schmidt, D. Müller, P. Mustakallio. LES simulation of the active chilled beam flow pattern, Roomvent 2014, Sao Paolo, Brazil, October 2014.

[3] P. Mathis, H. Freitag, V. Braunstein, D. Hegemann, J. Panaskova, M. Schmidt, D. Müller. Heat removal in shopping centers with high cooling loads by air-water systems with small fresh air amount and high cold water supply temperature, Ventilation 2015, Shanghai, China.

[4] M. Raffel, C. E. Willert, J. Kompenhans. Particle Image Velocimetry: A practical guide, Springer, New York, 1998.